Available online at www.sciencedirect.com

SciVerse ScienceDirect

Acta Materialia 60 (2012) 2497–2508

Acta MATERIALIA

www.elsevier.com/locate/actamat

# Delamination resistance of thermal barrier coatings containing embedded ductile layers

Matthew R. Begley [a,*], Haydn N.G. Wadley [b]

[a] Mechanical Engineering, University of California, Santa Barbara, CA 93106, USA
[b] Materials Science and Engineering, University of Virginia, Charlottesville, VA 22903, USA

Received 13 July 2011; received in revised form 22 December 2011; accepted 22 December 2011
Available online 1 March 2012

**Abstract**

Micromechanical models are developed to explore the effect of embedded metal layers upon thermal cycling delamination failure of thermal barrier coatings (TBCs) driven by thickening of a thermally grown oxide (TGO). The effects of reductions in the steady-state (i.e. maximum) energy release rate (ERR) controlling debonding from large interface flaws and decreases in the thickening kinetics of TGO are investigated. The models are used to quantify the dependence of the ERR and delamination lifetime upon the geometry and constitutive properties of metal/TBC/TGO multilayers. Combinations of multilayer properties are identified which maximize the increase in delamination lifetime. It is found that even in the absence of TGO growth rate effects, the delamination lifetime of TBC systems with weak TGO/bond coat interfaces can be more than doubled by replacing 10–20% of the ceramic TBC layer with a metal whose ambient temperature yield stress is in the ~100–200 MPa range.


*Keywords:* Thermal barrier coatings; Delamination; Metal layers

## 1. Introduction

Thermal barrier coating (TBC) systems are widely used to reduce the rate of oxidation and hot corrosion of internally cooled superalloy structures in gas turbine engines [1–4]. These coating systems consist of an aluminum-rich metallic bond coat (BC) applied directly to the superalloy component surface, a thin thermally grown oxide (TGO) that slowly forms on the BC surface during high-temperature exposure to oxygen, and an outer low thermal conductivity ceramic coating, such as ytrria-stabilized zirconia (YSZ) or gadolinium zirconate. This top coat reduces the temperature of the BC/TBC interface and slows the rate of oxidation. Thermal cycling in an oxygen environment eventually leads to spallation of the coating, usually by growth of an interface delamination crack [5,4,6], either at the TGO/BC interface or at the YSZ/TGO interface. These cracks are driven by the release of stored elastic strain energy associated with large compressive stresses that develop in the TGO upon cooling from the elevated temperature at which oxide growth occurs, as shown in Fig. 1. These stresses in the TGO have been extensively investigated by piezo-spectroscopic methods and have been shown to be primarily the result of thermal expansion mismatch between the TGO and other components of the system [7].

During high-temperature use, the TGO thickens parabolically with time, and the parabolic rate constant increases rapidly with temperature. The increase in TGO thickness can lead to a variety of complex failure mechanisms, with arguably two dominant modalities: (i) the stored elastic strain energy in the TGO/TBC bilayer drives large-scale debonding of the TGO/BC interface, with debond lengths much greater than the coating thickness, and (ii) the large stresses in the TGO and cyclic creep/plasticity in the BC lead to TGO rumpling (i.e. layer waviness), which induces locally high stresses that drive a variety of

* Corresponding author. Tel.: +1 8056791122.
*E-mail address:* begley@engr.ucsb.edu (M.R. Begley).

1359-6454/$36.00 © 2011 Acta Materialia Inc. Published by Elsevier Ltd. All rights reserved.
doi:10.1016/j.actamat.2011.12.039

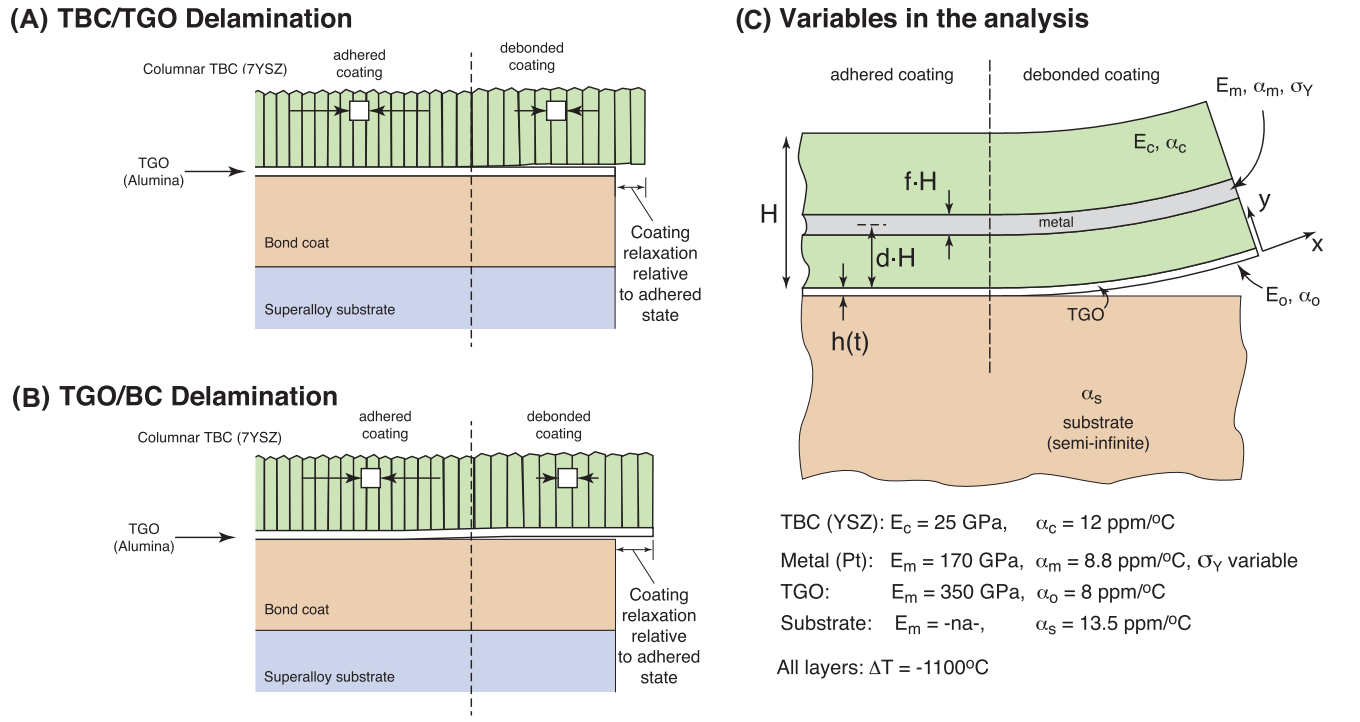


Fig. 1. Schematic illustration of the embedded metal layer concept. Two delamination scenarios are considered. (A) Failure above the TGO layer at the YSZ/TGO interface, in which case the TGO plays no role in debonding. (B) Failure beneath the TGO layer at the TGO/BC interface, in which case the TGO serves as the principle driving force for debonding. (C) Variables used in the analyses.

microcracking phenomena, notably cracking in the TBC near the crests and valleys of the rumpled TGO. Generally, both modalities are important: if rumpling can be suppressed, the initial microcracking that serves as the precursor to large-scale delamination is delayed, thus improving lifetimes. If the elastic strain energy in the TGO/TBC bilayer that is released by delamination is suppressed, greater TGO thicknesses are required for large-scale delamination. Thus, the central and critical role of the TGO has led to insightful studies of the complex interplay between many competing rate- and temperature-dependent phenomena that control TGO stress and morphology, with emphases on the creep-mediated interaction of the TGO with the BC (e.g. [4,6,8,9]), and microcracking or debonding near wavy interfaces (e.g. [10–12,14,13,15]).

These experiments and simulations have provided key insights that have led to proposed concepts for improvements to the BC to delay failure at the TGO/BC interface, i.e. the improvement of BC creep properties to reduce the rate of TGO rumpling, thus delaying or suppressing the formation of microcracks [16,17]. While improvements to BC creep have the desired effect of suppressing rumpling, continued alloy refinement is needed to ensure that BC oxidation behavior is acceptable [16]. In comparison to studies of BC behavior and cracking mechanisms in existing systems, relatively little attention has been directed at modifications to the ceramic TBC itself (i.e. the YSZ layer).

In this work, a micromechanical model is developed and used to explore the potential benefits of developing multilayered TBCs with the aim of delaying large-scale debonding, such as occurs after microcracks along an interface have coalesced into a dominant flaw (for which the delamination driving force is maximum). The principal goal is to present a simplified model that can be used by material developers to identify promising novel multilayer TBC systems that increase the critical TGO thickness (or, for example, a critical TBC modulus) necessary for large-scale delamination.

There are several reasons to believe that modifications to the TBC itself holds promise for suppressing large-scale debonding, at least for systems in which rumpling has been managed such that the time to reach criticality is dominated by oxide thickening (as opposed to rumpling). First, examination of the coefficients of thermal expansion (CTE) in Fig. 1C reveals that upon cooling from an elevated deposition temperature, elastic strain energy present in the TBC increases the driving force for delamination flaws. The in-plane elastic modulus in the TBC layer controls the strain energy in this layer. It has been shown that spallation can be significantly reduced by decreasing the modulus of the YSZ layer (by increasing its porosity) [18]. Since the elastic strain energy stored in the TBC layers can be released by delamination at the TBC/TGO interface, failure can occur at this interface even though the strain energy in the TGO remains fixed (see Fig. 1A). Secondly, it is important to note that the YSZ layer alters the kinetics of TGO growth by reducing the temperature of the TGO; however, it is a very ineffective diffusion barrier for oxygen and therefore does not reduce the oxygen flux to the TGO surface. Finally, reactions can occur between the ceramic

TBC and the TGO layer, resulting in the formation of "mixed-phase" regions at the interface, which can significantly reduce the TBC/TGO interface interfacial toughness, which promotes failure at this interface if the TBC modulus is high [19].

A recent experimental study has investigated the feasibility of inserting thin platinum layers into a YSZ coating to reduce the radiative component of heat transport to the TGO surface and thus its temperature [20]. However, this study revealed that the platinum layers also slowed the rate of oxide growth, perhaps by reducing the oxygen flux to the TGO. (Platinum has a very low oxygen diffusivity.) This increases the time necessary to reach a critical TGO thickness to drive spallation and thereby potentially improves coating lifetime.

The pure platinum metal layer used for these experiments has a low yield strength and significant ductility [21]. This mechanical response is quite different to that of the YSZ during cooling, and appears to offer several benefits. First, plastic deformation in the metal during cooling limits the amount of stored elastic energy in the layer (because of its low yield strength), potentially reducing the high stored elastic energy in the layers above the TGO. Second, if the stresses in the metal are tensile after coating delamination, they are balanced by compression in the YSZ layer and this lowers the amount of strain energy released during debonding. Third, plastic straining of the metal layer dissipates energy: a portion of the energy released by debonding would be dissipated by plastic work, as opposed to creating new interface crack area. It therefore appears possible that metal layers embedded within a ceramic layer might increase a coating's resistance to spallation by a number of mechanisms. However, the significance of the effects will depend sensitively upon the properties of the constituent materials and the coating architecture.

The micromechanical model presented here to evaluate the effects of embedding ductile layers in a ceramic TBC enables rapid identification of directions for future experimental assessments. The model allows for straightforward evaluation of the release of stored elastic energy and dissipated plastic work for debonding from a macroscopic interface flaw, which control the maximum energy release rate (ERR) for interface debonding. The model avoids the necessity of numerical (FEA) analyses that make broad parameter studies time-intensive and multilayer optimization very difficult. Naturally, the candidate systems and anticipated benefits identified with this model will require experimental study (such as those in Ref. [20]), to verify that the lifetime of the systems at hand are not dominated by the time required to develop a dominant interface flaw near interface features, such as rumples. Given that BC modifications continue to be explored, it is possible that a combination of new BCs and novel multilayers will ultimately extend lifetimes, by reducing the rate of rumpling and increasing the critical TGO thickness for large-scale delamination. The present model enables such a design study.

The impact of metal layers on TBC spallation lifetime is predicted by calculating the release of stored elastic energy and dissipated plastic work associated with the transition from the fully adhered to the debonded state. This calculation yields the ERR for steady-state debonding, i.e. that associated with an interface flaw that is much longer than the thickness of the multilayer. This ERR is the maximum possible for an interface flaw, and, in that sense, the model is conservative. The interface crack advances once the ERR reaches the interface toughness. The coating's time to failure can be estimated by calculating the time required to grow the TGO to the critical thickness that triggers this transition. This calculation can be extended to include the role of the metal layer in slowing the TGO growth rate.

Results are reported for the multilayer system and properties shown in Fig. 1C. The focus is on the effect of the yield strength, thickness and relative position of a single embedded layer upon the ERR relative to that of a reference ceramic coating. The model extends a previous study that analyzed a multilayer comprising a single ceramic coating with multiple embedded layers, placed symmetrically about the middle of the ceramic coating [22]. This previous analysis did not address (i) the effect of asymmetric metal layer placement, (ii) the effect of the TGO layer, or (ii) the retardation of the TGO growth rate. By explicitly addressing these factors here, the model presented here can be used to comprehensively explore potential improvements to coating lifetime and identify material combinations and layer architectures that increase coating lifetime.

## 2. Multilayer model

### 2.1. Overview

A schematic illustration of the model multilayer architecture to be analyzed here is shown in Fig. 1C. The TGO and TBC (YSZ) layers are assumed to be linearly elastic, while the embedded metal layer is assumed to be elastic–perfectly plastic, with a yield stress $\sigma_Y$. The general constitutive law for a given layer, denoted with subscript $i$, is assumed to be:

$$\epsilon_i = \frac{(1-v_i)\sigma_i}{E_i} + \theta_i(T,t) \tag{1}$$

where $E_i$ is the elastic modulus of the layer, $v_i$ is the Poisson's ratio, and $\theta_i(T,t)$ is a time- and temperature-dependent eigenstrain. The eigenstrain $\theta_i$ can be defined to represent thermal strains, intrinsic growth strains, etc., or to account for deposition stress (through suitable scaling with the modulus). For example, for thermal strains in a time-dependent problem, $\theta_i(T,t) = \alpha_i(T)\left(T(t) - T_i^o\right)$, where $\alpha_i(T)$ is the coefficient of thermal expansion (could be temperature dependent) of the $i$th layer and $T_i^o$ defines the reference temperature at which thermal strains are zero.

As will be illustrated, the problem is completely defined in terms of the eigenstrain $\theta_i$ values in the multilayer,

regardless of their physical source. In order to limit the number of parameters needed for the present examples, we assume the eigenstrains arise purely from thermal expansion mismatch, and the reference temperatures of all layers is the same, such that $\theta_i = \alpha_i \Delta T$, where $\Delta T$ is the temperature change of the system relative to a reference temperature free of thermal strain. Here, $\Delta T < 0$ corresponds to cooling from an elevated temperature. For many systems, relaxation at high temperatures implies that thermal strains are the dominant source of stress, and hence dominate the ERR predictions. It should be emphasized that alternative scenarios can be considered with the exact same model, with suitable definition of $\theta_i$. Finally, normalized results are presented relative to the base coating with no metal layers, further de-emphasizing the impact of specific properties chosen to define the eigenstrains.

The subscripts used to identify the layers are: $s$, substrate; $c$, TBC (e.g YSZ); $o$, TGO; and $m$, metal layer. The thickness of the TGO is defined as $h$, while the thickness of the TBC/metal multilayer is defined as $H$. The distance from the top of the TGO to the middle of the metal layer is defined as $d \cdot H$, while the thickness of the metal layer is defined as $f \cdot H$. Hence, $f$ defines the metal layer (volume) fraction in the TBC/metal multilayer coating.

Typical properties for a TBC system are given in Fig. 1C and are used as the basis for subsequent analysis, unless otherwise noted. Using these, the elastic stress in the embedded metal layer while it remains bonded to the substrate after cooling from the coating deposition temperature ($\Delta T \sim 1100\,^{\circ}\mathrm{C}$) is $\sigma_m \sim -500$ MPa. The negative sign indicates that the metal layer experiences a biaxial compressive stress and will yield upon cooling for the range of metal yield stresses considered here. Upon release of a multilayer by delamination at the TGO interface, the large compressive stresses in the multilayer relax, and the multilayers expand relative to the adhered state. During this debonding release, the metal can experience a reverse tensile plastic deformation, provided the metal yield stress is sufficiently low. The metal layer can therefore reduce elastic strain energy by two mechanisms, and both are addressed in the analysis below.

The model assumes that the superalloy substrate coated by the BC is homogeneous and of semi-infinite thickness. Thermally induced bending is therefore prevented when the layers are adhered, and the thermal strain of the substrate $\theta_s = \alpha_s \Delta T$ controls the adhered state's axial compression. To further simplify the analysis, it is assumed that all layers experience purely biaxial deformation even after debonding. Strictly speaking, if the delamination crack front remains straight, there is no loss of constraint in the debonded region since curvature about the $x$-axis is suppressed. While this effect is easily accounted for with an elastic analysis, preventing curvature about the $x$-axis leads to different plastic strains in the $x$- and $z$-directions, which significantly complicates a yielding analysis. The biaxial approximation is likely to be conservative since added constraint in the $z$-direction increases the stored elastic energy in the elastic layers of the debonded film and lowers the ERR for debonding (as compared to the biaxial case). The assumption of biaxial deformation implies that the results are only a function of the biaxial elastic modulus of the layers $\overline{E}_i = E_i/(1 - v_i)$. The bixaxial stress state implies that yielding occurs when the stress in the metal is $\sigma_m = \sigma_Y$, where $\sigma_Y$ is the uniaxial yield stress of the metal. It also implies that the yield strain $\epsilon_Y = \sigma_Y/\overline{E}_m = (1 - v_m)\sigma_Y/E_m$. With the biaxial assumption and this notation, the Poisson's ratios of the layers do not explicitly appear in the problem.

Debonding at either the YSZ/TGO interface or the TGO/substrate interface are both analyzed here. In the following, it is assumed that the critical ERR during crack growth at the relevant interface, $G_c$, is an intrinsic property of the interface and includes contributions from plastic deformation in the substrate. Hence, the influence of BC plasticity (possibly driven by thermal stresses) is accounted for by suitable modification of the assumed interface toughness. Crack growth occurs when the ERR $G \equiv \Delta W_e - W_p \geqslant G_c$. Here, $\Delta W_e$ is the change in stored elastic strain energy (per unit area) in going from the adhered state to the debonded state, and $W_p$ is the plastic work (per unit area) dissipated in the embedded metal within the YSZ coating during debonding. It is assumed that the plastic work dissipated in the embedded metal layer is dominated by relaxation of the thermal misfit strains ($\theta_i - \theta_j$), and is not influenced by the presence of the crack tip. That is, a ceramic layer shields the embedded layer from the elevated stresses near the crack tip, such that the crack tip fields do not induce significant additional plastic deformation in the embedded metal layer. This can be shown be rigorously true if $E_c G_c/\sigma_Y^2 < \Delta h$, where $\Delta h$ is the thickness of the TBC between the metal layer and the debonding interface. That is, if the distance over which the crack tip stress fields in the ceramic layer (adjacent to the BC) are elevated is much smaller than the distance to the metal layer, plastic deformation in the metal due to the crack tip will be much smaller than those arising from CTE mismatch. Put simply, if the above inequality is satisfied, the stiff ceramic layer between the interface and the embedded metal layer shields the metal layer from additional plasticity due to the crack tip. Again, it is worth emphasizing that while BC plasticity may have a profound effect, this is accounted for in present model through the definition of the critical interface toughness, with more ductile BCs presumably leading to a greater interface toughness.

The problem for the model defined above then consists of calculating the total axial stretch and curvature in the multilayer for a prescribed set of multilayer properties (modulus, thickness, etc.) and imposed thermal strains (e.g. $\theta_i = \alpha_i \Delta T$). Once these quantities are known for both the adhered and debonded states, one can compute the stored elastic strain energy and the plastic work dissipated in the metal layer, and, in turn, the ERR.

### 2.2. Governing equations

The following is an overview of the equations needed to predict the deformation, associated stresses and work terms necessary to compute the ERR. Although the resulting equations are straightforward algebraic relationships, the large number of parameters makes the full expressions unwieldy, and it is difficult to glean general insight from their complicated form. Since the full expressions are easily recovered with symbolic manipulation software such as Mathematica, we present only the essential elements of the analysis to convey the conceptual framework underpinning the computations. To aid in implementation, a more detailed derivation is included in Appendix A for the limiting condition where the deformation in the metal layer after debonding is fully plastic, in which case the resulting linear equations can be solved in closed form. Generally, the solutions are nonlinear and require numerical computations, due to the piecewise nature of the metal's elastic–perfectly plastic constitutive behavior.

The total strain as a function of vertical position in the multilayer is defined as $\epsilon(y) = \epsilon_o - \kappa \cdot y$, where $\epsilon_o$ is the total strain reference ($y = 0$) axis and $\kappa$ is the curvature of the reference axis, as shown in Fig. 1C. For elastic layers (the YSZ and TGO layers), the stress in the layers is also dependent upon the vertical position and is given by:

$$\sigma_i(y) = \overline{E}_i(\epsilon_o - \kappa \cdot y - \theta_i) \tag{2}$$

where $\theta_i = \alpha_i \Delta T$. In the metal layer, the stress is defined by its elastic–perfectly plastic response:

$$\begin{aligned}\sigma_m(y) &= \overline{E}_m(\epsilon_o - \kappa \cdot y - \theta_m - \epsilon^p) \quad \text{for } \sigma_m \leqslant \sigma_Y \\ &= \sigma_Y \cdot sign[\epsilon_o - \kappa \cdot y - \theta_m - \epsilon^p] \quad \text{for } \sigma_m > \sigma_Y\end{aligned} \tag{3}$$

where $\epsilon^p$ is the plastic strain at the start of the loading increment. If yielding occurs for a given $y$-position in the metal, then the stress is known and the plastic strains are calculated as $\epsilon^p(y) = \epsilon_o - \kappa \cdot y - \theta_m$.

The strain $\epsilon_o$ and the curvature $\kappa$ are determined by solving for the resultant axial force and resultant moment, which are zero in the absence of external loads:

$$\begin{aligned}N_r &= \sum_{i=o,c,m}\left(\int \sigma_i[\epsilon_o, \kappa, \theta_i, \epsilon^p, y]dy\right) = 0 \\ M_r &= \sum_{i=o,c,m}\left(\int \sigma_i[\epsilon_o, \kappa, \theta_i, \epsilon^p, y] \cdot y \cdot dy\right) = 0\end{aligned} \tag{4}$$

where the sum is performed over all layers in the multilayer being analyzed. A plastic strain contribution is only present for the metal layer. Substituting Eqs. (1) and (2) for the stresses in Eq. (3) results in two coupled nonlinear equations that can be solved for $\epsilon_o$ and $\kappa_y$, to determine the deformed state of the multilayer. Once these variables are determined, the stress throughout the multilayer is completely defined, and one can then proceed to calculate the stored elastic energy as follows.

While the multilayer coating remains attached to the substrate (i.e. prior to its debonding), the bending strain is zero ($\kappa = 0$) and the axial strain $\epsilon_o$ is equal to the thermal strain of the substrate; $\epsilon_o = \alpha_s \Delta T = \theta_s$ (since the substrate is assumed to be semi-infinite). This implies that the deformation is known, with layer stresses given by Eqs. (1) and (2). If $\theta_s < \theta_m$, the yield condition for the metal upon cooling from deposition, and associated plastic strains during cooling from deposition, are given by:

$$\theta_s - \theta_m \leqslant -\sigma_Y/\overline{E}_m \tag{5}$$

$$\epsilon_1^p = \theta_s - \theta_m + \sigma_Y/\overline{E}_m \tag{6}$$

(For cases with thermal mismatch of different sign, the signs of the following must be adjusted accordingly: see [22].) Since $\alpha_s > \alpha_m$ and $\Delta T < 0$, the metal will yield in compression and compressive plastic strains will be generated. The plastic strains due to cooling from the oxide growth temperature affect the subsequent deformation of the multilayer that debonds. With uniform stresses throughout the layers and $\epsilon_o = \theta_s$, the stored elastic energy in the adhered multilayer can be easily computed in closed form by integrating the strain energy density through the thickness of the multilayer.

After the multilayer debonds, Eqs. (1)–(3) are solved with $\epsilon^p = \epsilon_1^p$ (given in Eq. (5)) to determine $\epsilon_o$ and $\kappa$ for the released layer. (Note: if debonding occurs above the TGO, this layer is not included in the summation of Eq. (3).) The stored elastic strain energy in the released layer can again be found by integrating Eqs. (1) and (2) through the layers. The integrals for the elastic layers are straightforward to evaluate. For the elastic–perfectly plastic metal layer, the integration of elastic strain energy is computed by integrating $\sigma_m^2(y)/\overline{E}_m$, where the stress is given by Eq. (2): the piecewise nature of the stress–strain relation implies the stored elastic energy contribution will be $\sigma_Y^2/\overline{E}_m$ for those $y$-positions that have yielded. The plastic work dissipated in the metal during debonding is given by:

$$W_p = \sigma_Y \cdot \int \Delta\epsilon_2^p(y)dy \tag{7}$$

where $\Delta\epsilon_2^p$ is the plastic strain increment associated with release, which is a function of position in the metal film:

$$\Delta\epsilon_2^p(y) = 0 \ \epsilon_o - \kappa \cdot y - \theta_m - \epsilon_1^p \leqslant \sigma_Y/\overline{E}_m \tag{8}$$

$$= \epsilon_o - \kappa \cdot y - \theta_m - \epsilon_1^p - \sigma_Y/\overline{E}_m \ \epsilon_o - \kappa \cdot y - \theta_m - \epsilon_1^p \geqslant \sigma_Y/\overline{E}_m \tag{9}$$

Once again, note that these results apply when $\theta_s < \theta_m$: for other cases, the signs of the following equations must be adjusted accordingly (see [22]). If the metal yields upon debonding, it will yield in tension for $\alpha_s > \alpha_c > \alpha_m$; when the layer is released, the TGO and the coating expand (to recover a portion of the strains imposed by the substrate during cooling).

While the multilayer remains attached, the metal layer experiences a uniform stress state, given by either $\overline{E}_m(\theta_s - \theta_m)$ for the elastic case, or $\sigma_Y$ if yielding occurs. If the metal layer does not yield during debonding, or experiences complete through-thickness yielding, then the

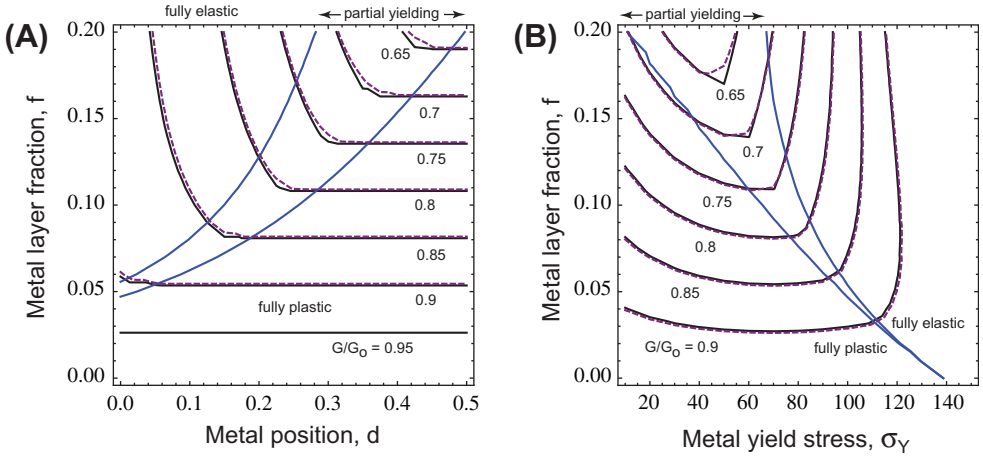


Fig. 2. Contour plots of the ERR $G/G_o$ for debonding at the YSZ/TGO interface, where $G_o$ is the ERR corresponding to a pure YSZ layer. (A) ERR contours for various metal layer fractions and positions with the metal yield stress $\sigma_Y = 75$ MPa; (B) ERR contours for various metal fractions and metal yield stresses with the position $d = 0.2$. For combinations between the blue lines, the metal experiences partial yielding. The dashed lines represent full numerical solutions to the piecewise linear problem. The solid lines correspond to solutions where the metal layer deformation is assumed to be fully elastic or fully plastic: in the partial yielding regime, the maximum ERR of these two solutions is plotted.

piecewise nature of its constitutive response is avoided, and closed-form analytical solutions are possible. Even in these limiting cases, the final expressions are cumbersome to present. A derivation of the analytical relationships is presented in Appendix A to aid in computer implementation.

The analytical solutions are also useful, since they approximate well the behavior of the multilayer for small volume fractions of metal. When the metal layer is thin in comparison to the TBC, gradients through the thickness are small, implying that the entire metal layer is likely to experience the same type of deformation (either completely elastic or completely plastic). The analytical solutions naturally enable quite rapid calculations, which is helpful when generating contour maps to highlight the interplay between specific layer properties. In the next section, a comparison between analytical and numerical solutions is presented first, to motivate the use of analytical solutions for subsequent results which would otherwise be computationally intensive.

## 3. Results

### 3.1. Delamination above the TGO

When delamination occurs above the TGO layer at the YSZ/TGO interface, the ERR during debonding is independent of TGO properties, since the TGO remains bonded to the semi-infinite substrate and this prevents the release of the TGO stress. Fig. 2 presents contour maps of the ERR as a function of metal layer fraction, position and yield stress: the ERR is normalized by $G_o = H\overline{E}_c(\theta_s - \theta_c)^2$, which is the stored elastic energy in an elastic ceramic coating of equal thickness. This also represents the ERR for a pure ceramic coating since debonding of a single layer relieves all strain energy (according to the biaxial deformation approximation discussed earlier). Values of $G/G_o$ less than unity represent a benefit from embedding a metal layer, and it is evident that significant reductions in debond driving force exist. For example, a multilayer with $f = 0.15$, located at $d = 0.2$ with a yield stress of $\sigma_Y = 75$ MPa has a 30% smaller driving force than a ceramic layer with the same total thickness.

The solid blue lines[1] indicate the boundaries where either the top or bottom of the metal film experience yielding during debonding, as predicted by an analysis that assumed only elastic unloading. Between the solid blue lines, the metal experiences partial yielding during debonding. Below the bottom solid blue line, the metal layer experiences complete yielding throughout its thickness during debonding. Above the top solid blue line, the metal layer remains completely elastic during unloading associated with debonding. In Fig. 2, the dashed lines represent the full non-linear solution as described in Section 2B. The solid lines represent the analytical approximation: in the regimes of complete yielding or complete elastic unloading, these should produce identical results to the complete nonlinear solution. Discrepancies in Fig. 2 outside the partial yielding zone are a result of numerical imprecision associated with solving and integrating piecewise-linear functions. In the partial yielding regime, the analytical result is defined as the maximum of the two ERRs obtained via the fully plastic and fully elastic analytical solutions. The results in Fig. 2 illustrate that this analytical approximation is quite accurate for small volume fractions: though not shown, results for larger layer fractions of metal show large discrepancies, as is expected since the through-thickness gradients of partial yielding play a larger role for thicker layers.

Fig. 2A indicates that when debonding involves complete yielding of the metal, the position of the metal layer has a

[1] For interpretation of color in Figs. 1–5, 7 the reader is referred to the web version of this article.

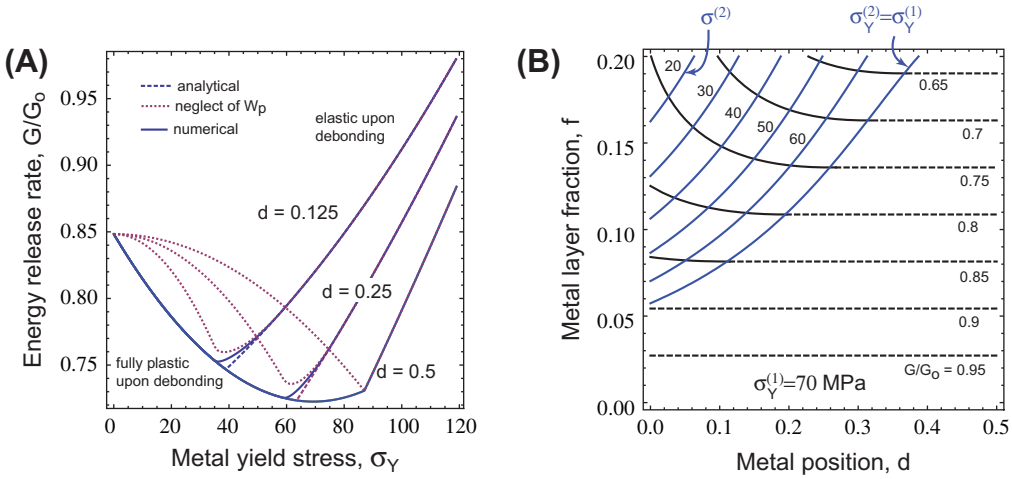


Fig. 3. (A) The ERR normalized by the result for a pure YSZ layer vs. metal yield strength for the volume fraction $f = 0.15$: the dotted lines illustrate predictions where the plastic work in the metal layer is neglected (i.e. just $\Delta W_e$). The solid lines are full numerical solutions, while the dashed lines represent the maximum of either the fully plastic or fully elastic analytical solutions. (B) Optimal value of yield stress that minimizes the ERR, and associated contours of $G/G_o$. The region with dashed lines corresponds to a constant yield stress ($\sigma_Y \sim 70$ MPa in this case), since the minimum occurs in the fully plastic regime and is independent of layer position.

negligible effect on the ERR and the reduction in $G/G_o$ due to the metal layer scales linearly with the layer fraction of metal. This implies that the earlier parameteric study [22] can guide multilayer design, since asymmetry in metal layer placement plays a small role. When debonding involves purely elastic unloading in the metal, the volume fraction plays a more significant role, and the ERR drops as the metal layer is positioned closer the TBC centerline. The latter effect arise because the maximum constraint on TBC expansion during debonding is achieved when bending is prohibited, i.e. when the metal/TBC multilayer is symmetric. Although not shown, results for $1/2 < d < 1$ are a mirror image of the contours in Fig. 2A, across a vertical axis. This is because the energy and work in the multilayer is independent of whether the metal is above or below the TBC centerline: whether or not the metal layer is above or below the centerline impacts the curvature of the debonded layer, and hence the mode-mixity of the interface crack. The latter effect is not considered here, though it could be critical for interfaces that exhibit strong dependence of the interface toughness on mode-mixity.

The lines in Fig. 2B have the same interpretation as those in Fig. 2A, with the regime of elastic unloading during debonding falling to the right, at higher levels of yield stress. For relatively low volume fractions, $f < 0.075$, the minimum ERR is independent of yield stress, provided it is sufficiently low to allow for complete yielding of the metal layer during debonding. At higher levels of metal volume fraction, the minimum ERR depends strongly on the yield stress. This is a result of two competing effects. If the yield stress is too low, the metal layer does not constrain expansion of the TBC, and the release of strain energy in the TBC during debonding is larger. Also, for low levels of yield stress, the dissipated plastic work during debonding is also low. Conversely, as the yield stress increases, plastic straining during debonding decreases and the elastic strain energy in the metal film (even when yielded) also increases.

Fig. 3A shows the dependence of $G/G_o$ upon metal layer yield strength for a single volume fraction and several different positions of the metal layer. The solid lines represent the full numerical solution, while the dashed lines represent the analytical solution described above (i.e. the minimum of the ERR predicted via fully elastic and fully plastic unloading). The dotted lines in Fig. 3A represent $\Delta W_e$, i.e. the ERR computed if one neglects the plastic work term. Clearly, the plastic work term plays a greater role for small yield stresses, since plastic strains can then be large. Note that as the yield stress goes to zero, the results asymptote to $G/G_o = 1 - f$, since the only effect of the metal is to eliminate the strain energy that would be stored in that layer if it were comprised of TBC material. Clearly, the partial yielding regime is rather small and well-approximated with the analytical results.

The presence of a minimum ERR in Fig. 3A has important implications for multilayer design, since it identifies an optimal value of yield stress that maximizes the reduction in ERR for a prescribed location in the multilayer. Given the relatively small discrepancy between the numerical and analytical results in the partial yielding regime, the analytical results can be used to accurately calculate the optimal value of $\sigma_Y$ and associated reduction in the ERR. As shown in Fig. 3A, the minimum occurs at either the minimum of the fully plastic solution ($d = 0.1$ in this case), or at the intersection of the fully plastic and fully elastic solutions ($d = 0.5$ in this case). Results for small volume fractions in Fig. 3B reveal that the transition to fully elastic unloading upon debonding is pushed to larger yield stresses: the reason for this is that for small volume fractions of metal, the TBC expansion upon release

overwhelms the metal layer and causes yielding even when the yield stress is comparatively high.

It is interesting to note that for the properties considered here, the dominant effect of the metal layer is to alter the stored elastic energy prior to debonding (by exploiting metal yield to reduce the strain energy in the adhered layer), and to alter the stored elastic energy in the debonded film (by exploiting metal yield to create tensile stress in the metal, which compresses the TBC and prevent the release of its energy). The results in Fig. 3 illustrate that the impact of plastic work is secondary (at least for the properties considered here), and plays a surprisingly minor role for configurations that minimize the ERR.

Fig. 3A reveals that the maximum reduction in ERR is obtained when the yield stress is the minimum of two values: the yield stress that minimizes the ERR assuming fully plastic behavior, or the yield stress associated with the transition from fully plastic to fully elastic behavior. The optimum yield strength for a plastic debonding solution, and associated ERR, is given by:

$$\sigma_Y^{(1)} = \frac{\overline{E}_m(\theta_c - \theta_s)}{4}$$
$$\frac{G^{(1)}}{G_o} = 1 - \left(1 + \frac{\overline{E}_m}{8\overline{E}_c}\right)\cdot f \qquad (10)$$

where these results reflect the asymptotic behavior of the fully analytical solution for $f \ll 1$ (i.e. neglect of $O[f^2]$ and higher.) Conversely, the optimum yield strength corresponding to the intersection of plastic and elastic debonding solutions, and associated ERR, is given by:

$$\sigma_Y^{(2)} = \overline{E}_m(\theta_c - \theta_s)\cdot\left(\frac{1}{2} - \frac{\overline{E}_m}{\overline{E}_c}\cdot(1 - 3(1-d)d)\cdot f\right)$$
$$\frac{G^{(2)}}{G_o} = 1 - f + f^2\cdot\left(\frac{\overline{E}_m}{\overline{E}_c}\right)^2(1 - 3(1-d)d) \qquad (11)$$

where again these results reflect the asymptotic behavior of the fully analytical solution for $f \ll 1$ (i.e. neglect of $O[f^2]$ and higher.) Fig. 3B illustrates the optimal value of yield stress and the associated ERR as a function of layer fraction and position. The transition from one optimal solution to the other occurs at $\sigma_Y^{(1)} = \sigma_Y^{(2)}$: to the left of this boundary, the optimal yield stress depends on both the layer fraction and the position. If the minimum occurs within the fully plastic range, the optimal solution is independent of the position, and the reduction scales linearly with volume fraction, as also supported by Fig. 2.

### 3.2. Delamination beneath the TGO

When debonding occurs beneath the TGO, the TGO layer plays two critical roles. First, the stiff TGO layer contains significant strain energy in the adhered state and this increases the strain energy released by debonding. Second, expansion of the stiff TGO layer upon debonding serves as an additional driving force for plasticity in the debonded section. The second of these effects is evident in the results shown in Fig. 4. It shows contour maps of the ERR as a function of metal layer position, volume fraction and yield stress, for a single value of TGO thickness. The ERR is normalized by the result for a pure YSZ layer on top of a 0.5 μm thick TGO layer. Comparing Fig. 4 to Fig. 2, one notes that the regime of fully plastic behavior is expanded to larger volume fractions of metal, and that results are no longer symmetric about $d = 0.5$. The reason for this is that stresses in the TGO increase the curvature of the multilayer after debonding: the stress in the metal layers increases with increasing proximity to the TGO. Though the reduction in the ERR due to the metal layer is approximately the same, it is important to note that $G_o$ is higher for cases in Fig. 4 than in Fig. 2, due to the presence of the TGO in the debonded stack.

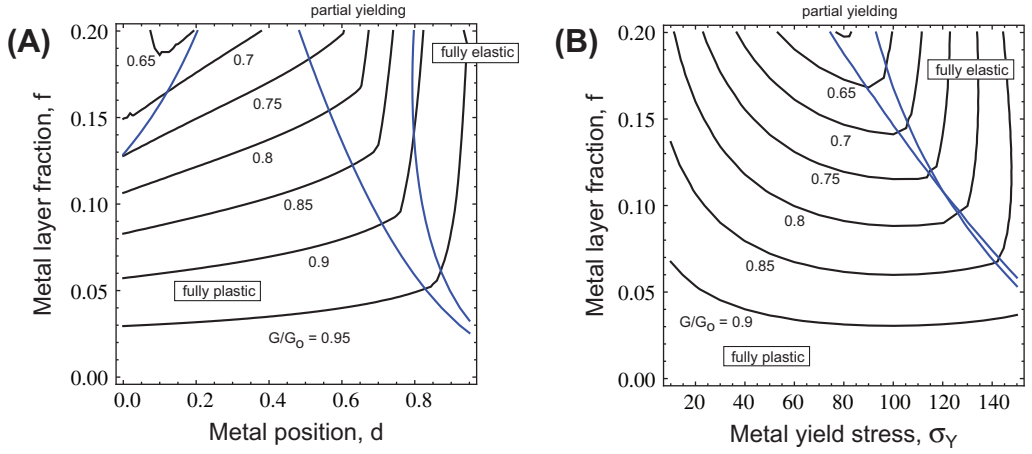


Fig. 4. (A) Contour plots of $G/G_o$ for debonding at the TGO/BC interface as a function of metal layer fraction and position, for at TGO thickness $h = 0.5$ μm and metal yield stress $\sigma_Y = 75$ MPa. (B) Contour plots of $G/G_o$ for debonding at the TGO/BC interface as a function of metal layer fraction and yield stress, for $d = 0.25$ and $h = 0.5$ μm. For combinations between the blue lines, the metal experiences partial yielding. The dashed lines represent full numerical solutions to the piecewise linear problem. The solid lines correspond to solutions where the metal layer deformation is assumed to be fully elastic or fully plastic: in the partial yielding regime, the maximum ERR of these two solutions is plotted. Comparing with Fig. 2, note the increase in the fully plastic regime due to the presence of the oxide layer, which drives plastic deformation.

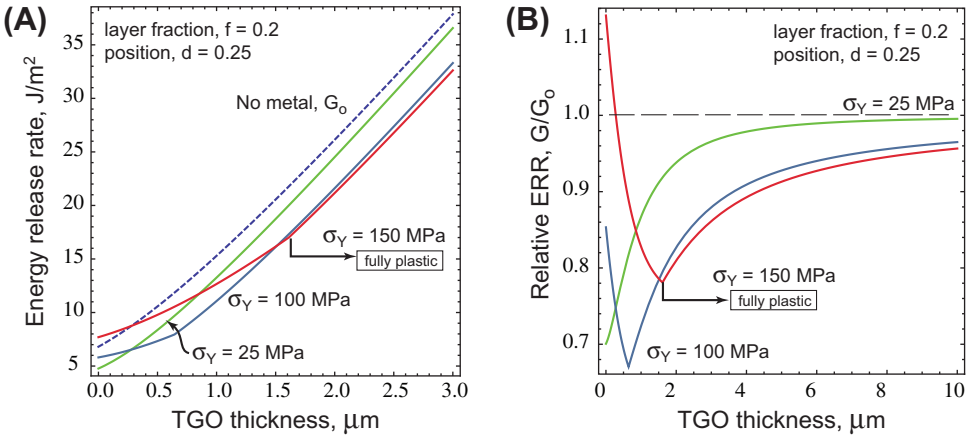


Fig. 5. (A) Energy release rate vs. oxide thickness, showing transitions from elastic debonding to fully plastic debonding. For small $h < 2$ μm, the ERR increases with $\sigma_Y$. However, the ERR decreases with yield strength in the thick TGO limit. (B) Normalized ERR vs. oxide thickness: the curves asymptotically approach unity, since for large oxide thickness the oxide dominates the energy released. Note there is a yield stress value that maximizes the critical oxide thickness: this value depends on the interface toughness.

The role of the TGO thickness is more clearly illustrated in Fig. 5, which plots the ERR as a function of TGO thickness in both its absolute and normalized form, for the position $d = 0.25$ and the volume fraction $f = 0.2$, and yield stresses in the range 25 MPa $< \sigma_y <$ 150 MPa. Note that at zero TGO thickness, the results correspond to those shown in Fig. 2. At low TGO thickness, the ERR is decreased by reducing the metal yield strength. For high levels of yield stress and small oxide thickness, the metal's behavior upon debonding is elastic (or partial yielding). Eventually, as the TGO thickness increases, the expansion of the TGO upon debonding is sufficient to cause complete yielding of the metal layer. In this regime, the ERR decreases with metal yield strength. In the asymptotic limit of thick TGO layers, the strain energy of the TGO dominates the results and the metal layer plays an increasingly minor role. As will be further discussed, this implies that metal layers will only be effective in extending lifetime for systems with relatively weak interfaces, which debond at relatively small TGO thickness.

The results in Fig. 5 illustrate that the potential benefit of the metal layers depends strongly on the critical ERR for debonding. For weak interfaces, say $G_c \sim 15$ J m$^{-2}$, the presence of the metal layer increases the critical TGO thickness for debonding by as much as 50%. Of course, this increase is only realized if the yield stress of the metal is sufficiently low: for elevated values of the yield stress, the elastic strain energy in the metal may elevate the ERR above that of a pure YSZ layer, such that debonding occurs prior to complete yielding of the metal. For a given layer fraction and interface toughness, there is an optimal value of yield stress that maximizes the TGO thickness at failure, and hence the time to failure of the interface.

For delamination driven by the increasing thickness of a TGO, the time to failure can be predicted by determining the critical TGO thickness for failure, $h_c$, and then using a time-dependent growth law for the oxide thickness to solve for the time at which $G[h_c] = G_c]$. In the following, the analytical solutions described earlier corresponding to either fully elastic or fully plastic behavior are used to predict $h_c$. (Because the maximum value of $G$ from these solutions accurately predicts the behavior even in the partial yielding regime, the minimum value of $h_c$ from these solutions accurately predicts the critical oxide thickness.) Previous studies have shown that (after a short transient behavior), the TGO thickness, $h(t)$, increases parabolically with time. This parabolic growth law can be written as:

$$h(t) = \sqrt{\beta \cdot t} \tag{12}$$

where $\beta$ is a parabolic rate constant that is governed by many factors, including the BC composition, the oxygen flux that arrives at the TGO surface and the temperature of the TGO. The incorporation of platinum layers in YSZ coatings has been shown to reduce the parabolic TGO thickening constant by up to a factor of 2. The fractional change in lifetime due to the embedded metal layers effect upon TGO thickening rate can be written as:

$$\frac{t_c}{t_c^o} = \frac{\beta_o}{\beta}\left(\frac{h_c}{h_c^o}\right)^2 \tag{13}$$

where $t_c^o$ is the critical time to failure in the absence of the metal layers, and $h_c^o$ is the critical thickness in the absence of the metal layers.

Fig. 6 illustrates lifetime gains as a function layer fraction, metal yield stress and the critical interface toughness; contours are shown for the ratio of the square of the critical thickness values with and without the metal layer. If a metal layer does not reduce the TGO thickening rate, these values represent the increase in lifetime due to the thermomechanical effect of the metal layers. If the metal layer does also change the rate of oxide growth, this effect is multiplicative with the results of the mechanics analysis: i.e. one multiplies the values in Fig. 6 by $\beta_o/\beta$, where $\beta_o$ is the growth constant in the absence of metal lines. The effect of a reduction in $\beta$ due to a metal layer can be significant. For a 100 μm thick YSZ layer on a NiCoCrAl-y BC, experiments [20] have

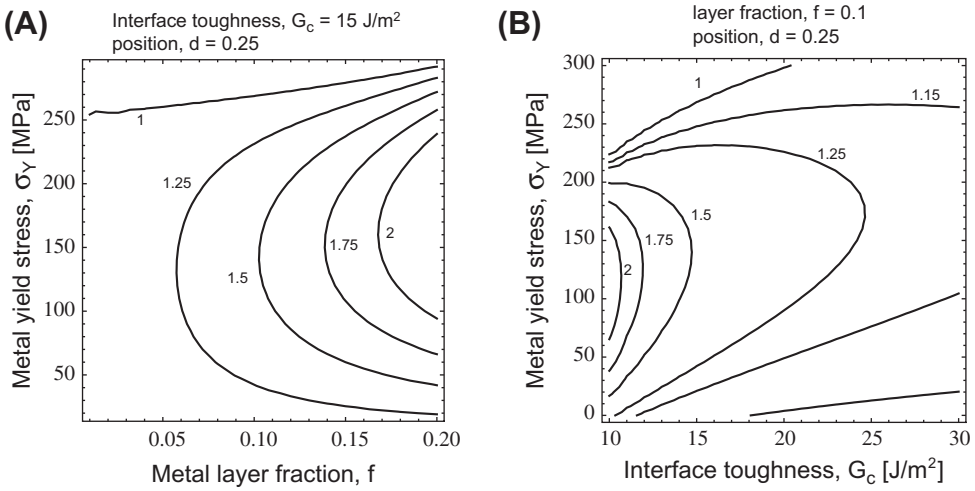


Fig. 6. Contour plots of the parameter $(h_c/h_c^o)^2$, where $h_c$ is the critical oxide thickness for multilayers with embedded metal and $h_c^o$ is the critical oxide thickness for a pure YSZ coating: for parabolic oxide growth, the gain in lifetime scales with $(\beta_o\beta)(h_c/h_c^o)^2$, where $\beta_o$ is the parabolic growth constant for the pure YSZ coating, and $\beta$ is the parabolic growth constant for the modified layer.

indicated that $\beta \sim 11\ \mu m^2\ h^{-1}$, while for a platinum/YSZ layer, $\beta \sim 8\ \mu m^2\ h^{-1}$. (It is believed that small voids in the metal layer eventually increase the effective oxygen transport rate over the (much lower) value predicted by diffusion through the fully dense metal.) As an example, the multiplicative effect of metal layer mechanics $h_c/h_c^o$ and slowing of the growth strains $\beta_o/\beta$ implies a doubling of spallation lifetime for volume fractions of $f \sim 0.1$ with $\sigma_Y \sim 150$ MPa.

The results in Fig. 6 clearly illustrate that the maximum gain in lifetime due to the presence of embedded metal layers arises when large volume fractions of the metals are used in systems with low values of interface toughness. Increasing the metal layer fraction increases the constraint afforded by the metal layer on TGO/YSZ expansion upon debonding. (The increase in plastic work due to increasing metal content is less dramatic, as suggested by Fig. 2.) The gain is largest for the smallest values of interface toughness: when the interface is weak, lifetimes are small, such that small increases critical thickness associated with the metal layers have a greater effect. Fig. 6 also indicates there is an optimal value of yield stress that maximizes the lifetime gain due to the presence of metal layers. This is a function of both the metal layer fraction and the interface toughness of the TGO/BC interfaces.

Fig. 7 plots the maximum gain in lifetime due to the presence of the metal layers, which is determined by finding the value of the yield stress that maximizes $h_c/h_o$. The associated optimal values of the yield stress are also shown. The values of the yield stress shown in Fig. 7 are much larger than the corresponding values in Fig. 3B for delamination of the YSZ/TGO interface: the reason for this is that the stiff TGO layer creates an additional driving force for plasticity during debonding, which allows for metals with larger yield stress to be utilized. Again, maximum benefit is achieved for weak interfaces, with as thick a metal layer as possible. Once again, it should be emphasized that the mechanisms of slowed oxide growth and mechanics of debonding are multiplicative, such that lifetime increases of 70% are possible with $f \sim 0.1$ (even for comparatively tough interfaces) provided $\beta_o/\beta \sim 1.3$ and $\sigma_Y \sim 180$ MPa.

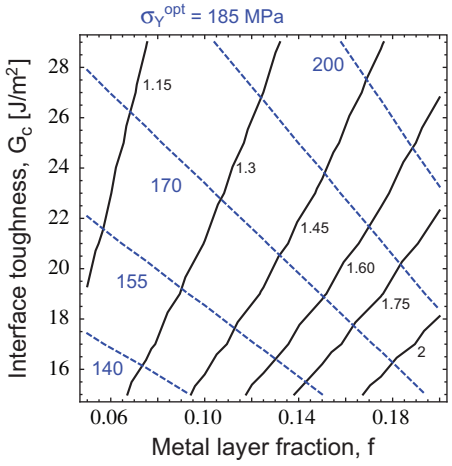


Fig. 7. Contour plots of the maximum possible value of $(h_c/h_o)^2$ associated with the optimal yield stress, and the optimal yield stress, as a function of metal layer fraction and interface toughness. For parabolic oxide growth, the gain in lifetime scales with $(\beta_o\beta)(h_c/h_c^o)^2$, where $\beta_o$ is the parabolic growth constant for the pure YSZ coating, and $\beta$ is the parabolic growth constant for the modified layer. (See text discussion.)

## 4. Summary

- The impact of embedded metal layers is greatest in TBC systems when the yield stress, position and volume fraction of the metal layer are such that complete yielding occurs during debonding. While an elastic–perfectly plastic analysis strictly requires the solution of nonlinear governing equations, the ERR is accurately predicted by the minimum predicted assuming either purely elastic or purely plastic deformation of the metal upon debonding. This allows derivation of closed-form analytical solutions that facilitate parameter studies.

- For debonding above the TGO which does then release its stored energy, the maximum reduction in ERR due to metal layers is insensitive to metal layer position provided the metal yields upon debonding: reductions in the ERR scale then scale as $f \cdot (1 + \overline{E}_m/(8\overline{E}_c))$, which implies reductions of $\sim 2f$ for porous thermal barrier coatings with relatively low modulus top coats. The dominant effect of the metal layer for such systems is to lower the strain energy while bonded and to serve as a constraint to TBC expansion during debonding: the effect of plastic work dissipated in the metal is secondary for such configurations. The optimal yield stress that minimizes the ERR in this regime is $\sigma_Y \sim 70$ MPa (for typical TBC properties) provided the metal layer is placed near the coating centerline. For metal layers placed closer to the TGO and layer fractions $f > \sim 0.05$, the optimal yield stress decreases with increasing layer fraction, to ensure that plastic deformation occurs during debonding.
- For debonding beneath the TGO, the high stiffness of the TGO and its considerable expansion upon debonding promotes plastic deformation in the metal, such that the fully plastic regime comprises a greater range of layer fractions and yield stress. The asymmetry introduced by the TGO in the debonded stack implies greater curvatures upon debonding, such that the metal layer position plays a stronger role in altering the ERR. The maximum reduction in the ERR occurs for relatively thin TGO layers, because thick TGO layers dominate the response: hence, metal layers have the greatest impact on TGO/BC delamination when the debond toughness is low.
- For debonding beneath the TGO, there is an optimal value of yield strength that maximizes the critical oxide thickness associated with failure for a given layer fraction and interface toughness. This yield strength lies in the range of 100 MPa le $\sigma_Y \leqslant 200$ MPa for $15 \leqslant G_c \leqslant 30$ J m$^{-2}$. and $0.05 \leqslant f \leqslant 0.2$. The reduction in TGO growth rate by metal layers has a mutiplicative effect upon that of the metal's thermomechanical behavior. Assuming a 30% reduction in TGO thickening kinetics, the predicted delamination lifetime improvements range from 50% to 300%, with the largest gain occurring for weak interfaces and with the highest layer fractions.
- The impact of the metal layer is greatest when the metal layer thickness is of the order of the TGO thickness; this implies that the greatest gains in lifetime are experienced for systems with relatively low toughness interfaces. For systems with tough interfaces, the critical oxide thickness for debonding can be large enough that the TGO dominates the response of the multilayer, and little benefit of a metal layer is seen.

## Acknowledgements

H.N.G.W. is grateful for support of this research by the Office of Naval Research, under Grant N00014-03-1-0297 (Dr. David Shiffler, Program Manager). M.R.B. is grateful for the support of the National Science Foundation, under grant CMII0800790.

## Appendix A

Here, we present a synopsis of the governing equations and solution steps for the following scenario. When the multilayer is attached, the metal layer experiences yielding in compression during cooling from elevated temperature, such that its stress state just prior to debonding is given by $-\sigma_Y$. During debonding, the elongation of the TGO drives complete reverse yielding in the metal layer, such that its stress in the released state is $\sigma_Y$.

After cooling from elevated temperature, the metal is presumed to yield and its stress is given by $-\sigma_Y$: the plastic strains generated in the metal layer are:

$$\epsilon_1^p = \theta_s - \theta_m + \frac{\sigma_Y}{\overline{E}_m} \tag{14}$$

The mechanical strains in the layers after cooling but while still adhered are then defined as:

$$\epsilon_c^m = \theta_s - \theta_c \tag{15}$$

$$\epsilon_o^m = \theta_s - \theta_o \tag{16}$$

The elastic strain energy in the multilayer while adhered is then computed from:

$$\Phi_1 = \int_{-h}^{0} \overline{E}_o \left[\epsilon_o^m\right]^2 dy + \int_{0}^{(d-f/2)H} \overline{E}_c \left[\epsilon_c^m\right]^2 dy + \int_{(d-f/2)H}^{(d+f/2)H} \frac{\sigma_Y^2}{\overline{E}_m} dy + \int_{(d+f/2)H}^{H} \overline{E}_c \left[\epsilon_c^m\right]^2 dy \tag{17}$$

where $h$ is the thickness of the TGO, $H$ is the total thickness of the metal/TBC multilayer, $d$ is the position of the center of the metal layer (as a fraction of the total layer thickness), and $f$ is the fraction of the metal/TBC multilayer occupied by the metal. Note that the usual factor of one-half is eliminated by the assumption of a biaxial stress-state.

After cooling and after release, the mechanical strains in the layers are defined as:

$$\epsilon_c^m = \epsilon_o - \kappa \cdot y - \theta_c \tag{18}$$

$$\epsilon_o^m = \epsilon_o - \kappa \cdot y - \theta_o \tag{19}$$

where $\epsilon_o$ and $\kappa$ describe the total elongation and curvature of the released multilayer. The axial force resultant and the moment resultant are computed from:

$$N_r = \int_{-h}^{0} \overline{E}_o \epsilon_o^m(y) dy + \int_{0}^{(d-f/2)H} \overline{E}_c \epsilon_c^m(y) dy + \int_{(d-f/2)H}^{(d+f/2)H} \sigma_Y dy + \int_{(d+f/2)H}^{H} \overline{E}_c \epsilon_c^m(y) dy \tag{20}$$

$$M_r = \int_{-h}^{0} \overline{E}_o \epsilon_o^m(y) \cdot y \cdot dy + \int_{0}^{(d-f/2)H} \overline{E}_c \epsilon_c^m(y) \cdot y \cdot dy + \int_{(d-f/2)H}^{(d+f/2)H} \sigma_Y \cdot y \cdot dy + \int_{(d+f/2)H}^{H} \overline{E}_c \epsilon_c^m(y) \cdot y \cdot dy \tag{21}$$

Note that if the metal layer is assumed to experience elastic unloading, one defines the mechanical strains in that layer as $\epsilon_m^m = \epsilon_o - \kappa \cdot y - \theta_m - \epsilon_1^p$, and replaces the yield stress terms in the above with $\overline{E}_m \epsilon_m^m(y)$. Absent any applied loads on the debonded multilayer, $N_r(\epsilon_o,\kappa) = 0$ and $N_r(\epsilon_o,\kappa) = 0$: hence, these two equations are solved to recover $\epsilon_o$ and $\kappa$, the deformation in the multilayer after debonding.

Once these are obtained, the strain energy in the debonded multilayer is computed using Eqs. (14) and (15) as follows:

$$\Phi_2 = \int_{-h}^{0} \overline{E}_o \left[\epsilon_o^m(y)\right]^2 dy + \int_{0}^{(d-f/2)H} \overline{E}_c \left[\epsilon_c^m(y)\right]^2 dy + \int_{(d-f/2)H}^{(d+f/2)H} \frac{\sigma_Y^2}{\overline{E}_m} dy + \int_{(d+f/2)H}^{H} \overline{E}_c \left[\epsilon_c^m(y)\right]^2 dy \quad (22)$$

Once again, note that if the metal layer is assumed to experience elastic unloading, one defines the mechanical strains in that layer as $\epsilon_m^m = \epsilon_o - \kappa \cdot y - \theta_m - \epsilon_1^p$, and replaces the yield stress terms in the above with $\overline{E}_m \left[\epsilon_m^m(y)\right]^2$.

The plastic strain *increment* associated with debonding, and the corresponding dissipated work are computed from:

$$\Delta\epsilon_2^p(y) = \left(\epsilon_o - \kappa \cdot y - \theta_m - \frac{\sigma_Y}{\overline{E}_m}\right) - \epsilon_1^p \quad (23)$$

$$W_p = \int_{(d-f/2)H}^{(d+f/2)H} \sigma_Y \cdot \Delta\epsilon_2^p(y) \cdot dy \quad (24)$$

The ERR is computed using the results from the above using:

$$G = \Phi_1 - \Phi_2 - W_p \quad (25)$$

where the last term is omitted if one is solving the case where the metal layer does not yield upon release.

## References


[1] Miller RA. Surf Coat Technol 1987;30:1.
[2] Levi CG. Curr Opin Solid State Mater Sci 2004;8:77.
[3] Stecura S. Thin Solid Films 1986;136:241.
[4] Evans AG, Mumm DR, Hutchinson HW, Meir GH, Pettit FS. Prog Mater Sci 2001;46:505.
[5] Spitsberg IT, Mumm DR, Evans AG. Mater Sci Eng 2005;394:176.
[6] Xu T, He MY, Evans AG. Interf Sci 2003;11:349.
[7] Tolpygo VK, Clarke DR. Acta Mater 2000;13:3283.
[8] Evans AG, He MY, Suzuki A, Gigliotti M, Hazel B, Pollock TM. Acta Mater 2009;57:2969.
[9] Balint DS, Hutchinson JW. J Mech Phys Solid 2005;53:949.
[10] Freborg AM, Ferguson BL, Brindly WJ, Petrus GJ. Mater Sci Eng A 1998;245:182.
[11] Busso EP, Lin J, Sakurai S, Nakayam M. Acta Mater 2001;49:1515.
[12] Busso EP, Lin J, Sakurai S. Acta Mater 2001;49:1529.
[13] Aktaa J, Sfar K, Munz D. Acta Mater 2005;53:4399.
[14] Busso EP, Qian ZQ. Acta Mater 2006;54:325.
[15] Busso EP, Wright L, Evans HE, McCartney LN, Saunders SRJ, Osgerby S, et al. Acta Mater 2007;55:1491.
[16] Tryon B, Murphy KS, Yang HY, Levi CG, Pollock TM. Surf Coat Technol 2007;202:349.
[17] Carroll LJ, Feng Q, Pollock TM. Metall Mater Trans A 2008;39:1290.
[18] Hass D, Parrish PA, Wadley HNG. Curr Opin Solid State Mater Sci 1998;8:77.
[19] Zhao H, Begley MR, Heuer A, Sharghi-Moshtagin R, Wadley HNG. Surf Coat Technol 2011;205:4355.
[20] Yu Z, Zhao H, Wadley HNG. J Am Ceram Soc, 2011; 94: 2671.
[21] Ioginov YN, Yermakov AV, Grohovskaya LG, Studenak GI. Platinum Metals Rev 2007;4:178.
[22] Begley MR, Wadley HNG. J Am Ceram Soc 2011;91:S96.